PCCP

PAPER

View Article Online
View Journal | View Issue

Cite this: *Phys. Chem. Chem. Phys.*, 2024, **26**, 3857

Site specifically probing the unfolding process of human telomere i-motif DNA using vibrationally enhanced alkynyl stretch†

Tiantian Dong,[ab] Pengyun Yu,[ab] Juan Zhao[ab] and Jianping Wang*[ab]

Received 2nd November 2023,
Accepted 2nd January 2024

DOI: 10.1039/d3cp05328h

rsc.li/pccp

The microscopic unfolding process of a cytosine-rich DNA forming i-motif by hemi-protonated base pairs is related to gene regulation. However, the detailed thermal unfolding mechanism and the protonation/deprotonation status of site-specific cytosine in DNA in a physiological environment are still obscure. To address this issue, a vibration-enhanced C≡C probe tagged on 5′E terminal cytosine of human telomere i-motif DNA was examined using linear and nonlinear infrared (IR) spectroscopies and quantum-chemistry calculations. The C≡C probe extended into the major groove of the i-motif was found using nonlinear IR results only to introduce a minor steric effect on both steady-state structure and local structure dynamics; however, its IR absorption profile effectively reports the cleavage of the hemi-protonated base pair of C_1–C_{13} upon the unfolding with C_1 remaining protonated. The temperature mid-point (T_m) of the local transition reported using the C≡C tag was slightly lower than the T_m of global transition, and the enthalpy of the former exceeds 60% of the global transition. It is shown that the base-pair unraveling is noncooperative, with outer base pairs breaking first and being likely the rate limiting step. Our results offered an in-depth understanding of the macroscopic unfolding characteristics of the i-motif DNA and provided a nonlinear IR approach to monitoring the local structural transition and dynamics of DNA and its complexes.

1. Introduction

Cytosine-rich sequences can fold into an intercalated four strand i-motif structure *via* hemi-protonated base pairs ([C–H–C]$^+$) under weak acidic or even neutral conditions and unfold into a hairpin-like or a random-coil structure under basic conditions or at high temperature. Both the conformation transformation process and structure stability of i-motif DNA are related to the transcription, gene regulation and genomic function in biological systems.[1–5] The i-motif structure has also been widely used in biotechnology, drug delivery, molecular switching and nanostructure construction because of its unique proton-induced folding/unfolding properties.[6,7] The structural stability and the conformational dynamics of the folding/unfolding of the i-motif DNA are of great significance for gene regulation[8,9] as well as for molecular device fabrication.[6,7,10,11] The folding and unfolding process of the i-motif is known to be both pH and temperature dependent, and reversible.[12] The kinetics of the folding/unfolding of the i-motif DNA has been an important research topic, and has been studied by using several methods, such as nuclear magnetic resonance (NMR) spectroscopy, circular dichroism (CD) spectroscopy, fluorescence resonance energy transfer (FRET) and surface plasmon resonance (SPR) spectroscopy.[13–18] Time-resolved spectroscopy and molecular dynamics simulations have been recently used to explore the detailed mechanism steps of the folding/unfolding and the asymmetric structures of hemi-protonated base pairs, as well as the characteristics of protonation–deprotonation of related bases.[14,16,19–21]

Using stopped-flow circular dichroism (SFCD) spectroscopic measurements, a pH induced unfolding model involving two steps of neutralization of protons was proposed, in which the rate-limiting step was found to be preferably the cooperative neutralization of two of the totally six protons.[16] This work was supported by all-atom molecular dynamics simulations.[20] Although there have been extensive works on the pH-induced

[a] *Beijing National Laboratory for Molecular Sciences, Molecular Reaction Dynamics Laboratory, CAS Research/Education Center for Excellence in Molecular Sciences, Institute of Chemistry, Chinese Academy of Sciences, Beijing, 100190, P. R. China. E-mail: jwang@iccas.ac.cn; Fax: (+86)-010-62563167; Tel: (+86)-010-62656806*

[b] *University of Chinese Academy of Sciences, Beijing 100049, P. R. China*

† Electronic supplementary information (ESI) available: Synthesis of ^{TIPS}EdC phosphoramidite; MS characterization of the C≡C-labeled DNA strand; CD spectra of the unlabeled and C≡C-labeled DNA strands; FTIR spectra of nucleosides with band assignment; temperature-dependent FTIR difference spectra; plot of the C≡C band frequency position *vs* intensity; temperature-dependent FTIR spectra of ^{TMS}EdC and ^{TMS}EdC$^+$; fitting results of van't Hoff function; location of the six adenines in the i-motif DNA; comparison of the unlabeled and C≡C-labeled strands monitored by the pump–probe spectra; nonlinear IR results of the unlabeled and C≡C-labeled strands at pH* 7.6; and the fitting results of the population relaxation dynamics. See DOI: **https://doi.org/10.1039/d3cp05328h**

folding/unfolding pathways of the i-motif structure, temperature-induced folding/unfolding dynamics are much less studied. Molecular dynamics simulations were carried out at higher temperature to reveal the conformation of stable intermediates in the deprotonated state during the thermodynamic unfolding period of the i-motif DNA.[21] Recently, it was shown by temperature-dependent infrared measurements that for thermal unfolding, the outer hydrogen bonds involving C(2)=O(2) and N(4)H_2 amino groups break first, subsequently followed by the breaking of the hydrogen bond involving $N(3)^+$.[22] However, the microscopic mechanism and pathway of the unfolding of the i-motif DNA, particularly the site-specific protonation/deprotonation status of a given nucleobase is still under debate.

Vibrational spectroscopy has shown excellent sensitivity to biomolecular conformation and has been a suitable tool to study protein and DNA structural transition dynamics.[23–27] An external vibrational probe tagged on a biomolecule with its vibrational absorption outside the major absorption regions of the biomolecules has become a very useful method for site-specific monitoring.[28–31] Recently, phenylacetylene was used as a Raman tag to report the protonation/deprotonation status of a nucleobase in the folded- and unfolded-states of the i-motif DNA.[32] In our recent work, we have explored a novel vibrationally enhanced alkynyl probe with a single absorption band that has excellent sensitivity for the local structure of nucleobases and their solvent environment, as well as the hydrogen-bonding interaction between the nucleobases and solvent.[33] Since no new polar short-range interaction is introduced by the alkynyl group, the interpretation of the observed IR spectra can be easily carried out. Because of this, it is advantageous to be used for monitoring site-specific and local structures and dynamics of DNA as well as tracking the forming and breaking events of the nucleobase pairs, and the protonation/deprotonation status of the nucleobases. To this end, the extent of perturbations of the extrinsically tagged IR probe to the local structure is an important and complicated issue that determines the applicability of the probe and the reasonability of the obtained experimental results. As will be seen from the FTIR spectral results in this work, the externally tagged probe shows little effect on the equilibrium structure of the i-motif DNA. However, several studies pointed out that an apolar methyl group or polar hydroxymethyl group tagged on cytosine may alter its local hydration and base pairing dynamics, as well as structure flexibility.[34–36]

In this work, we use infrared spectroscopy employing a vibrationally enhanced alkynyl probe tagged on the site-specific nucleobase of hTelo i-motif DNA (PDB:1EL2, as illustrated in Fig. 1a) to monitor the thermally unfolding process and the protonation–deprotonation properties of the selected nucleobase. Herein, the alkynyl probe is triisopropylsilylacetylene (TIPSE) and the alkynyl probe modified deoxycytidine is ^{TIPS}EdC.[33] The C≡C probe was tagged on the 5′E terminal cytosine (C_1) by the conventional solid-phase DNA synthesis method[37] to track the status of the C_1–C_{13} nucleobase pair during the unfolding process of the i-motif DNA.

The structure of the TIPSE-labeled (named as C≡C-labeled) i-motif strand is displayed in Fig. 1b, and the chemical structure of the IR probe is shown in Fig. 1c. We carried out temperature-dependent FTIR experiment for both unlabeled and C≡C-labeled strands. The transition temperature (T_m) derived from the C≡C stretch for the local transition was found to be slightly lower than the global transition temperature, indicating that the cleavage of outer at least the terminal base pair involving the C_1–C_{13} base pair is likely to be one of the initial steps of the unfolding and may also be the rate-limiting step. For C_1, it remains to be protonated during the unfolding of the i-motif DNA. Detailed analysis is given in this work.

In addition, the extent of perturbations to the local structure and solvation dynamics from the externally tagged C≡C probe was explored in both the unlabeled and C≡C-labeled strands using ultrafast nonlinear IR spectroscopy including two-dimensional IR (2D IR) spectroscopy. The extrinsic C≡C probe tagged to C_1 was found to have a minor perturbative effect on the local structure dynamics, solvent dynamics, and structural flexibility of the i-motif DNA.

2. Experimental and methods

2.1. Sample preparation

The hTelo i-motif DNA is a 22 (nucleotides, nt) oligomer with the sequence of 5′-CCCTAACCCTAACCCTAACCCT-3′,[38] however, U_7

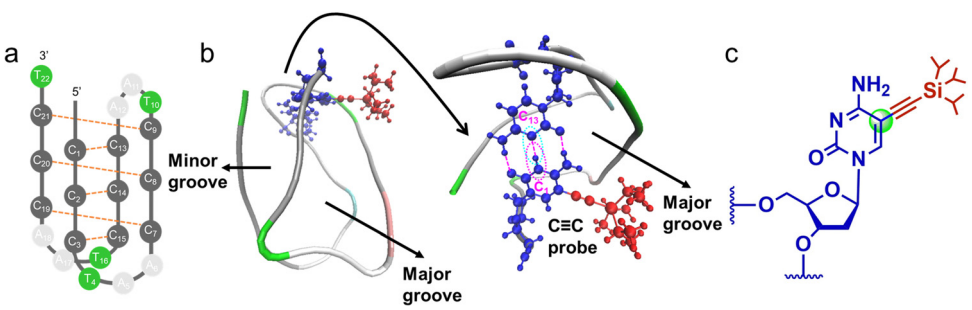

Fig. 1 (a) A scheme of the intercalated, four-stranded hTelo i-motif DNA structure. The sequence is marked with letter C (cytosine), T (thymine), A (adenine) and number subscript. (b) Illustration of the C≡C probe (red marker) labeled C_1 nucleobase of the hTelo i-motif DNA strand in the folded structure. Straight-line arrows indicate the major and minor grooves of the i-motif structure. The i-motif structure frame is showed in the residue colored tube model. Hemi-protonated base pair of C_1–C_{13} is highlighted in blue and hydrogen bonds are displayed with a colored dashed line. (c) Chemical structure of the C≡C probe labeled C_1 nucleobase.

of 1EL2 was replaced by C_7 in this work. The C≡C labeled C_1 strand is 5′-^{TIPSE}CCCTAACCCTAACCCTAACCT-3′. Both unlabeled and C≡C-labeled strands were synthesized by the Suzhou Biosyntech Co., Ltd. The TIPSE modified deoxycytidine phosphoramidite (^{TIPS}EdC phosphoramidite) was prepared in this work using the conventional phosphosamidite synthesized method.[37] The synthetic details and NMR characterizations are shown in Scheme S1 and Fig. S1–S5, ESI.† The MS spectrum of the C≡C labeled strand is shown in Fig. S6 (ESI†) to show that the C≡C group has been labeled on the i-motif strand. Powdered samples were at default purity and centrifuged twice at a speed of 10 000 rpm for 10 minutes. Then all labile protons of the two samples were exchanged in deuterium oxide (D_2O) three times. The prepared buffer D_2O solution is pH* 7.6 Dulbecco's phosphate-buffered saline (DPBS buffer solution) with the pH* value adjusted by deuterium chloride (DCl). pH* refers to the uncorrected (for D_2O) pH-meter reading value at 25 °C. Both unlabeled and C≡C-labeled strands were dissolved in pH* 4.5 DPBS buffer solution at a concentration of 10 mM for temperature-dependent FTIR measurement and ultrafast nonlinear infrared spectroscopic measurement.

2.2. Methods

Temperature-dependent FTIR spectra were recorded using a commercial Nicolet 6700 FTIR spectrometer with an attached homemade temperature-controlling device for samples. Sample solutions were held in a double-sample-cell holder with a half-cell sample solution and a half-cell solvent (DPBS buffer solution). The FTIR spectra of the two samples were collected from 25 °C to 90 °C, with a step of 5 °C. Each spectrum is solvent background subtracted.

Ultrafast nonlinear IR spectroscopy was used to characterize the structure dynamics of the unlabeled and C≡C-labeled strands in the 6-μm wavelength region. 2D IR spectra of the two samples were collected using a pulse-shaped 2D IR apparatus.[39,40] Briefly a laser of 800-nm center wavelength, 3-mJ pulse energy, 25-fs pulse width, and 1-kHz repetition rate generated using a commercial Ti-sapphire laser amplifier was modulated into the needed mid-infrared pulse (center frequency of 1740 cm^{-1}) through an optical parametric amplifier (OPA) and a difference frequency generator (DFG). The out pulse is split into two pulses, one is called the pump pulse, passing a series of IR optics, entering the pulse shaper, and generating a pair of delay time (*i.e.*, the coherence time, τ) adjustable pump pulses, the other is called the probe pulse, passing the IR polarizer and half-wave plate and entering the IR monochromator along the same direction as the generated nonlinear IR signal. Detection frequency (ω_t) is defined by the IR monochromator and grating. The delay time between the paired pump pulses and the probe pulse is called the waiting time (T_w). The 2D IR signal was collected in the pump–probe geometry at each of a series of T_w. Additionally, the magic-angle IR pump–probe spectroscopic measurement was carried out using the same experimental setup with the 54.7 degree between the laser electric-field directions of the pump pulse pair (at τ = 0) and the probe pulse.

Quantum chemistry calculations were performed using the density functional theory (DFT + D3) at the level of B3LYP by Gaussian 09,[41] in which the D3 dispersion correction scheme calculates the inter- and intramolecular dispersion interactions that are useful for large (supramolecular) systems by employing the given system coordinates (and atomic numbers). The 6-311+G** basis set was used for geometry optimization of the protonated/non-protonated cytosine and nucleobase pair structures, followed by IR spectral simulations. Even though the size of the model dimer systems (≤91 atoms) considered in this work is not too large, the dispersion correction on DFT is still considered in our computation.

3. Results and discussion

3.1. Temperature-dependent FTIR spectroscopy

Both the unlabeled and C≡C-labeled strands are in the folded state (i-motif structure) when dissolved in pH* 4.5 DPBS buffer solution at room temperature (25 °C) as illustrated using the CD spectra (shown in Fig. S7, ESI†). Temperature-dependent FTIR spectra of the unlabeled and C≡C-labeled strands are shown in Fig. 2. In the 6-μm wavelength region, the vibrational absorption is mainly from three nucleobase's vibration modes which could reflect the global folding/unfolding process of the i-motif DNA. The spectral evolution of the C≡C-labeled strand is consistent with that of the unlabeled strand. Each band is assigned with colored shading and marked with a combined letter-number in Fig. 2a and b, among which, C is cytosine, T is thymine, and A is adenine. With increasing temperature, the C1 band (1665–1655 cm^{-1}) frequency gradually red shifts and intensity gradually increases. The A1 band (1625 cm^{-1}) behaves similarly. In the 1700–1750 cm^{-1} region, the C^+1 (C^+ is the protonated cytosine) band intensity decreases whereas the C^+1' band intensity increases, in which one isosbestic point appears at 1707 cm^{-1} (marked by a black star). In a thermal transition, an isosbestic point may appear between a new band and a vanishing old band, which can be used as an indicator of phase transition and can reveal the transition temperature (mid-point of the structure transition).[42–46] Therefore, both the unlabeled and C≡C-labeled strands have changed from the folded state (i-motif structure) to the unfolded state (random coil) at the temperature ranging from 25 °C to 90 °C, as indicated by the temperature-dependent FTIR spectra. This process seems like a typical two-state transition. As seen in Fig. 2a and b, there seems to be a transition point around 60 °C (drawn in a colored dotted line), at which all band frequencies or/and intensities especially the C1 band and pair of C^+1/C^+1' peaks change most drastically.

Comparing the unlabeled and C≡C-labeled strands, the characteristics of key spectral changes and their temperature dependencies are quite similar for the two samples. This indicates that the external C≡C probe tagged on C_1 has little effect on the steady-state i-motif structures and transformation between structures, even though the label has a relatively large terminal group (TIPS). This is probably because the probe

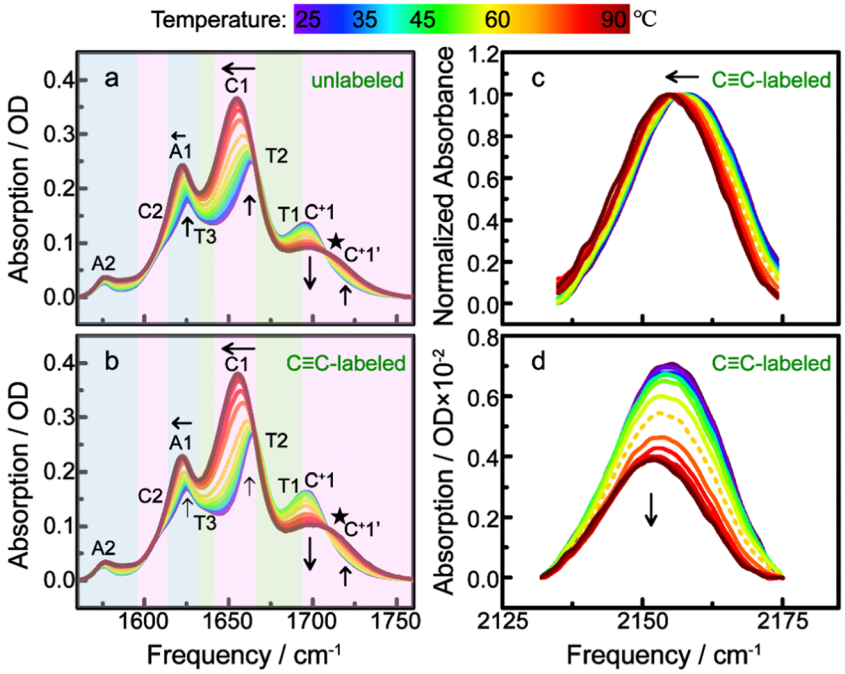

Fig. 2 Temperature-dependence of the FTIR spectra of the unlabeled (a) and C≡C-labeled (b) h-Telo i-motif DNA strand in pH* 4.5 DPBS buffer solution in the 6 μm wavelength region collected from 25 to 90 °C. The C≡C stretching absorption region of the intensity normalized (c) and baseline corrected (d) spectra of the C≡C-labeled strand. Colored shadings indicate the contribution of three nucleobases to the spectra and each peak is marked with the combined letter-number in (a) and (b). Arrows indicate the directions of changes of peak intensity gain/loss and frequency shift with increasing temperature. The dotted line of the 60 °C spectrum in each panel indicates the case near thermal unfolding transition temperature. Black star in (a) and (b) indicates the isosbestic point.

extends toward into the major groove of the i-motif structure and TIPS is far enough from the main bulk structure (Fig. 1b). This point has been reported by our recent work of the C≡C probe.[33] Hence the TIPS group yields only a minor steric effect on the local structure of the i-motif DNA studied here.

The stretching vibration peak of C≡C tagged on C_1 also changed gradually as displayed in Fig. 2c and d. The peak position red shifts, and intensity decreases as a function of temperature, indicating that this label can sense the unfolding process of the i-motif DNA, in particular the C_1–C_{13} base pair cleavage process as indicated in Fig. 1b. The C≡C spectral change also gave a transition mid-point temperature of around 60 °C, as shown by the dotted spectral line in both Fig. 2c and d. Therefore, the temperature dependence of the C≡C band could reveal the thermally unfolding process of the i-motif DNA and the local structure transition involving C_1–C_{13} base pair cleavage. However, two issues should be pointed out. The first is the components of the C≡C band. From the folded-state to the unfolded-sate, the C≡C band red shifted about 4 cm^{-1}. It is feasible but unnecessary to split the C≡C band into two or more peaks representing the absorption components for different states, because this would complicate spectral interpretation. Instead, the C≡C band could be treated as a whole in which as the unfolded component increases, the absorption of the lower-frequency component increases and the overall C≡C band red shifts. The second is the incompleteness of the C≡C band line shape shown in both Fig. 2c and d, which is due to the presence of both OD stretching vibration and bending-libration combination absorption bands of D_2O that interacts with the higher-frequency peak wings of the C≡C band. Baseline corrected spectra are shown in Fig. 2d.

The IR absorption peaks in the 6-μm region were further used to characterize the unfolding process especially for making a distinction between the global transition and local transition processes. We collected the IR spectra of three nucleosides (dA, dT and dC) and protonated dC (dC^+) at room temperature, which are shown in Fig. S8a (ESI†). The vibrational absorption band of each base of the unfolded i-motif structure (random coil) shown in Fig. 2a and b is very close to that of the free nucleoside monomer. The superposed spectrum of nucleosides' monomer spectra with the ratio (4 : 6 : 6 : 6) shown in Fig. S8b (ESI†) nearly coincided to the spectra of the unfolded i-motif strand shown in Fig. 2a. The 6-μm bands of i-motif DNA strand were further assigned based on the assignment of nucleoside monomers, which are marked similarly in the two figures. Peak assignment of the protonated/deprotonated cytosine in both the folded and unfolded forms is crucial, because the hemi-protonated base pair breaking involves cytosine, whose IR signature changes dramatically whereas those of the A and T bases only change slightly during the unfolding of the i-motif DNA.

From the folded to unfolded (random coil) structure of the i-motif, the C=O stretching vibrational absorption frequency of cytosine (band C1) shifted from 1664 cm^{-1} to 1655 cm^{-1} as base pairs break and the π–π base-pair stacking degrades. The change of the C1 band is directly related to the structural

transformation and reflects the global unfolding process. Protonated cytosine (dC^+) of the folded-state has an IR peak located in 1709 cm^{-1}, which is shown in Fig. S8a (ESI†). As temperature increases, the concentration of the folded component decreases whereas the unfolded component increases. This is reflected by the intensity of the C^+1 band at 1696 cm^{-1} (folded state) that decreases, and by that of the C^+1' band at 1720 cm^{-1} (unfolded state) that increases.

The frequency assignment of these two bands is consistent with previous reports.[26,47] Specifically, Wieser's group indicated that a new absorption band at 1694-cm^{-1} is the unique feature for the intercalated structure forming,[47] whereas a recent work of the Tokmakoff group pointed out that the growth of the 1720 cm^{-1} band indicates a gain of the protonated cytosine in the random-coil state.[26] Therefore, the changes in the paired C^+1/C^+1' bands can be used to reflect the global unfolding process in this work. In addition, two shoulder bands appeared near 1689 cm^{-1} and 1667 cm^{-1} corresponding to thymine carbonyl stretch (T1 and T2 in Fig. 2a and b) which are consistent with dT's absorption shown in Fig. S8a (ESI†). A shoulder band near 1637 cm^{-1} corresponds to the thymine ring vibration (T3 in Fig. 2a and b), while the shoulder near 1609 cm^{-1} corresponds to the ring mode of cytosine (C2 in Fig. 2a and b). The 1625-cm^{-1} and 1575-cm^{-1} peaks correspond to the ring modes of adenine (A1 and A2 in Fig. 2a and b). These band assignments are listed in Table S1 (ESI†).

3.2. Two-state model

To determine the transition temperature (T_m), the temperature dependence of selected spectral parameters (band frequency and intensity) is fitted with a sigmoidal function derived from the two-state model:[22,48]

$$y(T) = a + bT + \frac{\Delta a + \Delta bT}{1 + \exp\left(\frac{\Delta H}{R}\left(\frac{1}{T} - \frac{1}{T_m}\right)\right)}, \quad (1)$$

where $y(T)$ is the spectral parameter to be fitted, a and b are the parameters describing the linear dependence of $y(T)$ under the transition, Δa and Δb are the fluctuations of parameters a and b during the transition, T_m is the transition midpoint, R is the ideal gas constant, and ΔH is the enthalpy. The enthalpy ΔH for the unfolding is the van't Hoff enthalpy at T_m.[49–51]

The C1 band frequency andintensity, C^+1' band intensity, and C≡C band frequency and intensity were fitted to the two-state model, and fitting curves are shown in Fig. 3. For the C1 band intensity, the intensity growth of 1653 cm^{-1} (unfolded state) in the difference spectra (shown in Fig. S9, ESI†) was used, in which each spectrum was subtracted from that at 25 °C. Fitting the C1 band frequency (Fig. 3a) yielded a T_m value of 62.7 °C and 63.2 °C for the unlabeled and C≡C-labeled strands, respectively. Fitting the C1 band intensity yielded a T_m value of 62.9 °C and 63.0 °C, respectively, for both strands as shown in Fig. 3b. The growth of the C^+1' band was also fitted to give the T_m values of 62.8 °C and 63.0 °C, respectively, for both strands as shown in Fig. 3c. The red shift of the C1 band, the growth of the 1653-cm^{-1} band and that of the C^+1' band are all related to the six hemi-protonated base pair cleavage process which is linearly correlated with the concentration of the random coil structure. The global transition mid-point of C≡C-labeled strand (*i.e.*, 63.1 °C on average) is found to be

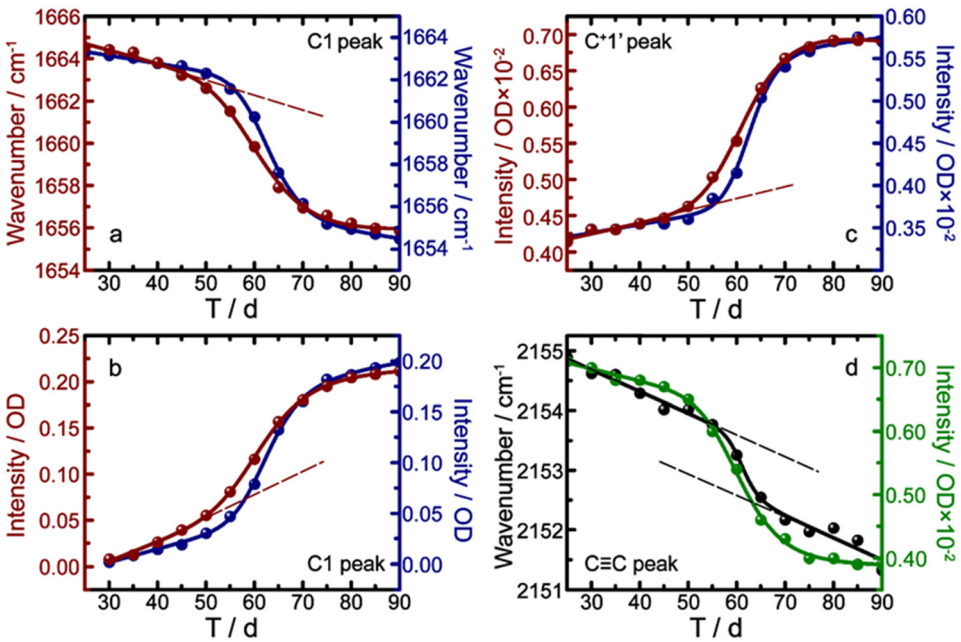

Fig. 3 Thermal unfolding curves of the unlabeled strand (wine line) and the C≡C-labeled strand (navy line) monitored by linear IR spectroscopy at (a) 1664 cm^{-1} (C1 band) frequency shift, (b) 1653 cm^{-1} (C1 band) intensity increase from the difference spectrum, and (c) 1720 cm^{-1} (C^+1' band) intensity increase. (d) 2155 cm^{-1} (C≡C stretch) frequency shift (black line) and intensity decrease (green line) for the C≡C-labeled strand. Solid line represents least-square fitting to the two-state unfolding transition.

only 0.3 °C higher than that of the unlabeled strand (*i.e.*, 62.8 °C on average). The transition temperature region of the C≡C-labeled strand is slightly narrower than that of the unlabeled strand as indicated in Fig. 3a–c. These results illustrate that the C≡C-labeled strand is slightly more stable than the unlabeled strand, indicating that the external probe has little perturbation in the steady-state structure of the i-motif DNA including the folded, partially folded and unfolded structures. The global T_m determined in this work is slightly higher than previously reported T_m from a 21 nucleotide (nt) strand (*i.e.*, 59.5 °C) by CD spectroscopy[32] and is slightly lower than previously reported T_m from a 24 nt strand (*i.e.*, 66.2 °C)[52] under similar conditions.

The temperature dependence of C≡C band frequency was also fitted with the two-state model and yielded a T_m value of 61.2 °C (shown in Fig. 3d with a black curve). Moreover, fitting temperature dependence of the C≡C band intensity yielded a T_m value of 61.5 °C (shown in Fig. 3d with a green curve). The relationship between the C≡C band's red shift and its intensity loss appears to be linear (Fig. S10, ESI†), suggesting that both of them are related to the C_1–C_{13} base pair breaking and the local site denaturation. The T_m derived from the C≡C stretch presents the local transition mid-point. Significantly, the local transition mid-point given by the C≡C stretch (*ca.* 61.4 °C on average) is smaller than that of the global transition mid-point (*ca.* 63.1 °C on average). The difference is *ca.* 1.7 °C. Hence it is believed that the hemi-protonated base pairs of C_1–C_{13} breaking precede the global denaturation, and are perhaps among the initial steps of base pair breaking during the thermal unfolding.[16] The unfolding pathway may include an initial transition phase that is associated with the partial unfolding of the base pairs or possibly one of the outer/terminal base pairs before the remaining structure unfolding.

The non-cooperativity of base pairs results in a broad distribution of segments with different cleavage of base pairs, which may tilt the initial denaturation curves in the lower-temperature region (as illustrated in Fig. 3a–c), but does not form a new sigmoidal transition yet.[53] As shown in Fig. 3d (black dotted line), at the initial transition stage, the C≡C stretching frequency shifts on the basis of a large slope which significantly deviates from the two-state model. This is reasonable because the C≡C band would shift significantly only when the hemi-protonated base pair C_1–C_{13} breaks. The linear shift of the initial transition stage is probably due to the C_1–C_{13} base pair weakening along with the degradation of the i-motif structure as temperature increases. At the ending stage of the transition, the red shift of the C≡C band is not completely linear but fluctuates, which is probably due to the temperature effect.

To examine the temperature effect on the C≡C stretch, we carried out T-dependent FTIR spectroscopy of C≡C-labeled protonated and non-protonated cytosine dissolved in the DPBS buffer solution, respectively. Because of the low solubility of ^{TIPS}EdC dissolved in DPBS buffer solution, ^{TMS}EdC instead of ^{TIPS}EdC to be used for FTIR measurements here. The T-dependent spectral parameters of the 6-μm region and C≡C stretching region of ^{TMS}EdC and ^{TMS}EdC$^+$ are shown in Fig. S11 (ESI†). As illustrated in Fig. S11c (ESI†), the C≡C stretch of ^{TMS}EdC had a linear red-shift with a total shifted wavenumber of 3 cm^{-1}. As illustrated in Fig. S11d (ESI†), the C≡C stretch of protonated ^{TMS}EdC$^+$ had a fluctuated red-shift with a total shifted wavenumber of 2 cm^{-1}. As illustrated in Fig. S11b (ESI†), the 1714 cm^{-1} band of protonated ^{TMS}EdC$^+$ had a fluctuated blue-shift with a total shifted wavenumber of 1 cm^{-1}. It can be seen that the temperature effect does induce the 6-μm region or C≡C band shifting with a small range of wavenumber but not a two-state model. Given the experimental uncertainty, it is not clear that the temperature induced frequency shift is meaningful or not. Therefore, the temperature effect is ignored in this work. The changes of C≡C stretch and the 6-μm region with increasing temperature mainly reflected the structure transformation of i-motif DNA. To further examine the C≡C stretch of the protonated or non-protonated state, the pH-dependent spectra of the C≡C stretch of ^{TMS}EdC was collected and shown in Fig. S11a (ESI†). The C≡C stretch of protonated ^{TMS}EdC$^+$ blue shifted by 10 cm^{-1} and was much weaker than that of non-protonated. In addition, the C≡C stretch red-shifting by a wavenumber of 5 cm^{-1} induced by i-motif structure unfolding in this work is very nearly to that amount of ^{TMS}EdC induced by the hydrogen-bonding interaction of a protonic solvent.[33] This further illustrated that the changes of the C≡C stretch mainly reflected the hydrogen bonding forming/breaking process of the C_1–C_{13} base pair. The temperature dependent frequency change of the monomer shown in Fig. S11d (ESI†) is a purely temperature-induced frequency redshift of the C≡C stretching mode, which could be another source of the tilted frequency change observed in Fig. 3d.

3.3. Thermodynamic parameters

To obtain the thermodynamic parameters (enthalpy ΔH_m^{vH}, entropy ΔS_m and free energy ΔG_m) at T_m for global transition and local site transition from the equilibrium melting dynamics, we used the van't Hoff approach to plot ln K *vs.* $1/T$ as follows:

$$\ln K = \Delta H_m^{vH}/RT + \Delta S_m/R, \quad (2)$$

$$\Delta G_m = \Delta H_m^{vH} - T\Delta S_m \quad (3)$$

here, we evaluate the equilibrium constant K as a function of fraction of i-motif/single strand:

$$K = [\text{single strand}]/[\text{i-modif}] = (\text{Fraction single strand})/(1\text{-Fraction single strand}), \quad (4)$$

where the fraction of single strand *vs.* temperature is extracted from the IR intensity at 1653 cm^{-1} for both the unlabeled and C≡C-labeled cases. And that of local unfolding is extracted from the frequency shift of the C≡C stretching mode:

$$\text{Fraction single strand} = (IR_T - IR_{25\,^\circ C})/(IR_{90\,^\circ C} - IR_{25\,^\circ C}), \quad (5)$$

where IR_T is the IR intensity at temperature T, $IR_{25\,^\circ C}$ is that at 25 °C, and $IR_{90\,^\circ C}$ is that at 90 °C. The van't Hoff fitting curves

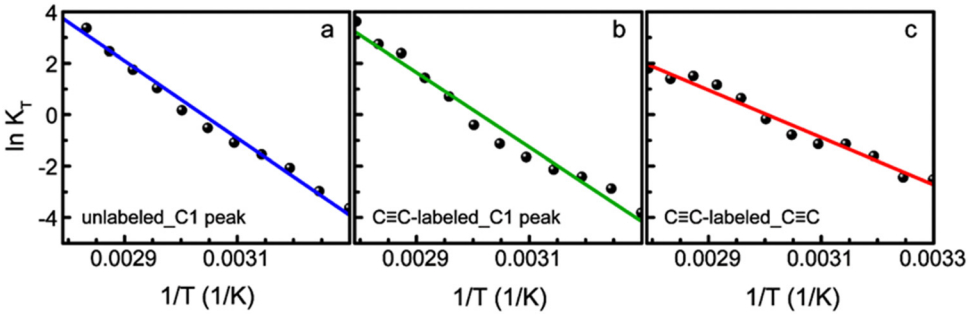

Fig. 4 The van't Hoff plot derived from the C1 band intensity at 1655 cm^{-1} for the unlabeled strand (a) and the C≡C-labeled strand (b), and the C≡C stretch band frequency shift for the C≡C-labeled strand (c).

for three cases are shown in Fig. 4. The fitting thermodynamic parameters are very close to the previously reported results[52,54,55] and are all collected in Table S2 (ESI†). The difference between the reported results and our results is mainly due to the sequence difference of i-motif and may also be due to difference of experimental conditions including ionic strength and pH.

The values of ΔH_m^{vH}, ΔS_m and ΔG_m for the local-site transition (18.30 kcal mol^{-1}, 0.055 kcal mol^{-1} and −0.12 kcal mol^{-1}) determined using the C≡C probe were smaller than those for the global unfolding (28.75 kcal mol^{-1}, 0.087 kcal mol^{-1} and −0.37 kcal mol^{-1}). However, each thermodynamic parameter for the local-site transition accounts for 30–60% of the global unfolding transition for the C≡C-labeled strand.

The comparison of thermodynamic parameters between the global and local unfolding processes is very important. According to Wadkins work,[54] the melting enthalpy of one C–C^+ breaking in the i-motif DNA was approximately 5.0 kcal mol^{-1} while the melting enthalpy of the local site involving C_1–C_{13} breaking was approximately 18.3 kcal mol^{-1} based on the van't Hoff fitting results of the present work. Even taking into account the experimental error, the melting enthalpy of the C_1–C_{13} pair breaking is still much larger than that of an usual C–C^+ breaking in the i-motif DNA and exceeds 60% (=18.30/28.75) of total melting enthalpy. The free energy ΔG_m of the local site C_1–C_{13} breaking accounts 30% of the total melting free energy for the C≡C-labeled strand at T_m. These results suggest that the initial step of the C_1–C_{13} breaking is very likely to be in the rate-liming step as it has a larger energy barrier than the rest of the base pairs to be broken when there are two or more steps of unfolding.[56,57] It should be pointed out that the local site transition enthalpy derived from the C≡C probe does not present explicitly the melting enthalpy of C_1–C_{13} breaking but may correspond to the enthalpy change involved in the C_1–C_{13} breaking under the global unfolding process. Thus, whether the C_1–C_{13} breaking is in the rate-liming step or not still requires more experimental evidence such as the unfolding rate obtained from time-resolved temperature-jump spectroscopy.[57]

The global transitions (Fig. 3a–c) and the local site transition (Fig. 3d) fitted by the two-state model yielded a slightly lower T_m but a quite larger enthalpy for the former, suggesting that the local site involving C_1–C_{13} breaks first, followed by the outer base pair breaking, or that the rate-limiting step includes at least the C_1–C_{13} breaking.

The global transition of six base-pair breaking is found to be not completely cooperative but rather shows a two-state transition behavior. According to the above results, we proposed a thermal unfolding model for the i-motif DNA:

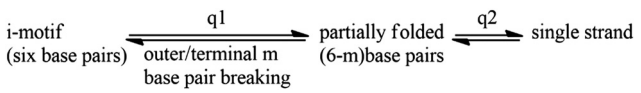

(6)

Here, the first step is the rate-limiting step in which outer m base pairs of the six base pairs (including at least the terminal base pair of C_1–C_{13}) break first. The local transition enthalpy exceeds 60% of the total transition enthalpy. The calorimetric enthalpy change equals van't Hoff enthalpy change ΔH_m^{vH} within experimental errors in the two-state process.[58] Here q1 ≫ q2 is predicted in the unfolding path shown above. The unfolding of the remaining base pairs occurs relatively rapidly.

This model is mechanically consistent with the reported pH-induced unfolding model[16] and the results from high-temperature molecular dynamics simulations.[21] Although there is no comparative experiments on the C≡C probe tagged on other nucleobase sites, we speculate that the local transition T_m of other sites is unlikely to be smaller than that of the terminal site (C_1–C_{13}) involved this work, and the local transition ΔH_m^{vH} of other sites is unlikely to exceed 50% of the total. This suggests that the breakings of these base pairs are non-cooperative. Based on this model, we believe that the initial step of the C_1–C_{13} breaking is very likely to be in the rate-liming step.

3.4. Simulated IR spectra

To further explore the mechanism of the peak frequency and intensity change in the C≡C stretching mode induced by the C_1–C_{13} breaking, and to understand the asymmetric feature of the hemi-protonated base pairs under the thermal unfolding transition, we carried out DFT calculations on the C≡C stretching mode of different cases involving the C≡C-labeled hemi-protonated dimer and protonated/non-protonated deoxycytidine monomer. The optimized structures and the corresponding simulated IR spectra of the C≡C stretching mode are

shown in Fig. 5. Our recent work showed that a limited solvent effect on the C≡C stretching frequency of ^{TMS}EdC,[33] and considering the location of the C≡C moiety in the labeled bases, we carried out frequency calculations of the C≡C stretching mode in the gas phase.

The calculated frequencies were scaled by a factor of 0.967.[59] Here, dC$^+$ is protonated dC and ^{TIPS}EdC$^+$ is protonated ^{TIPS}EdC. Two C≡C-labeled hemi-protonated dimers are considered: ^{TIPS}EdC$^+$-dC and ^{TIPS}EdC-dC$^+$. From Fig. 5b–e, one sees that only the case of changing from ^{TIPS}EdC$^+$-dC to ^{TIPS}EdC$^+$ (Fig. 5b) shows certain agreement with the experimental results (Fig. 3c and d) in both the frequency red shift and the intensity decrease of the C≡C stretching mode. In contrast, the calculated C≡C stretching intensity greatly increased from ^{TIPS}EdC$^+$-dC to ^{TIPS}EdC (Fig. 5e), which is not what was observed experimentally. Moreover, the C≡C stretching band may red shift significantly (about 10 cm^{-1}) when ^{TMS}EdC$^+$ is deprotonated as illustrated in Fig. S11a (ESI†). Hence, the observed red shift of the C≡C stretching band (*ca.* 10 cm^{-1}) induced by the deprotonation of cytosine is much larger than that induced by the unfolding transformation (about 5 cm^{-1}). This infers that base C_1 is unlikely to be deprotonated under the thermal unfolding transition of the i-motif.

The C≡C band red shifts as the hemi-protonated base pair C_1–C_{13} breaks. The C≡C band intensity is quite low in the protonated cytosine (in the unfolded state) as indicated by the IR spectrum of ^{TMS}EdC$^+$ (not shown), but is slightly larger when the hemi-protonated base pair of C_1–C_{13} is formed (in the folded state). The vibrational intensity of the C≡C stretch of both unfolded and folded but protonated C_1 is weaker than that of the non-protonated C_1. In addition, as illustrated in Fig. 5c and d, the C≡C stretching mode is either intensity increased or frequency blue-shifted from ^{TIPS}EdC-dC$^+$ to ^{TIPS}EdC or to ^{TIPS}EdC$^+$, which does not agree with the experimental results. This infers that the proton localization may more likely occur at residue C_1 than C_{13} in the hemi-protonated base pair of C_1–C_{13} in which a delocalized proton is known to oscillate between the two wells.[19] However, there has been no proof about the tendency of proton delocalization in C_1–C_{13}.[19] Thus, the C≡C probe used here has successfully tracked the protonation status

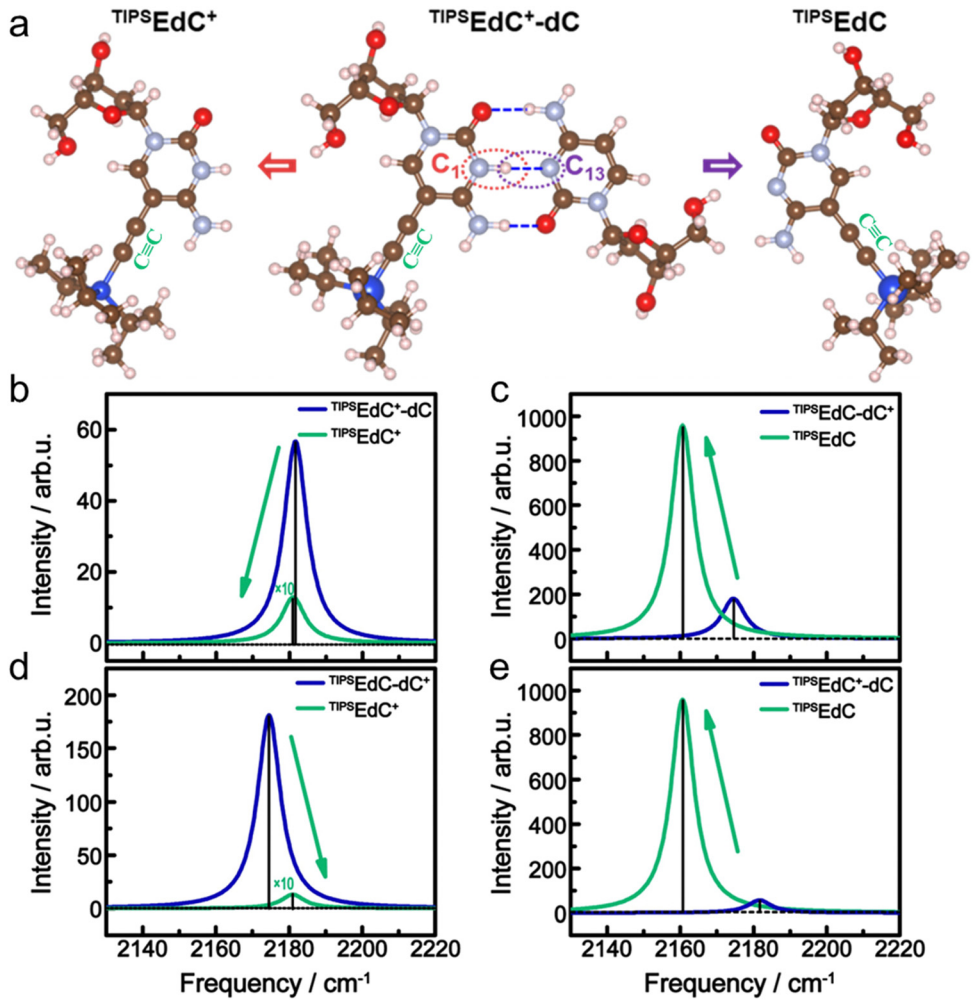

Fig. 5 (a) Illustration of the hemi-protonated base pair of the folded state (middle), and the protonated monomer (left) and non-protonated monomer (right) of the unfolded state. Simulated IR spectra of ^{TIPS}EdC$^+$-dC *vs.* ^{TIPS}EdC$^+$ (b), ^{TIPS}EdC-dC$^+$ *vs.* ^{TIPS}EdC (c), ^{TIPS}EdC-dC$^+$ *vs.* ^{TIPS}EdC$^+$ (d) and ^{TIPS}EdC$^+$-dC *vs.* ^{TIPS}EdC (e). The intensity is enlarged by ten times for ^{TIPS}EdC$^+$ in (b) and one hundred times in (d).

of the C_1–C_{13} pair during the unfolding process of the i-motif DNA.

It should be noted that the chemical environment of the C≡C-labeled C_1–C_{13} hemi-protonated base pair located on the i-motif structure in the DPBS buffer solution is more complicated than that of a single nucleoside or paired nucleosides. The labeling group faces outward the base-pairing region of the i-motif DNA, being a few covalent bonds away from the hydrogen bonds, so that the hydrogen-bonding effect on the C≡C stretching frequency is indirect and thus not significant. To examine the effect of non-covalent interactions, including mainly the van der Waals interaction and hydrophobic interaction, between the C≡C-labeled C_1–C_{13} and nearby bases and associated chemical groups, we visualize the PDB structure of hTelo i-motif DNA[38] in Fig. S13 (ESI†). It is shown that the estimated distance between the C≡C-label and C_2 base, or between that and the A_{12} base, is 6.06 Å or 13.57 Å. Thus, the non-covalent interactions between the C≡C probe and these two nearby groups are considered to be weak and are not considered specifically in our model calculations shown in Fig. 5. Other interactions, such as the possible π–π stacking effect, may also influence the C≡C stretching frequency to some extent, but are considered specifically in the calculation of our work.

3.5. Probe perturbations

The extent of perturbations of the extrinsically tagged probe in the local structure and solvation dynamics is examined using 2D IR and pump–probe spectroscopies and the results are shown in Fig. 6.

Time-dependent and purely absorptive 2D IR spectra of the folded-state with unlabeled strands (top row) and those of the C≡C-labeled strands (bottom row) are shown in Fig. 6a. Paired diagonal peaks, which are composed of positive peaks (red) coming from the $v = 0 \rightarrow v = 1$ transitions (v is vibrational quantum number) and negative peaks (blue) coming from the corresponding $1 \rightarrow 2$ transitions are shown. Off-diagonal cross peaks (coming from vibration mode coupling or energy transfer) are also shown, for example between C1 and T1 modes (Fig. 6a). Three prominent diagonal peaks in the 2D IR spectra are observed at 1625 cm^{-1}, 1665 cm^{-1} and 1689/1696 cm^{-1}, which are attributed to the A1, C1 and T1/C^+1, respectively, as shown in the FTIR spectra (Fig. 2). There is almost no difference in the 2D IR line shape between the C≡C-labeled strand

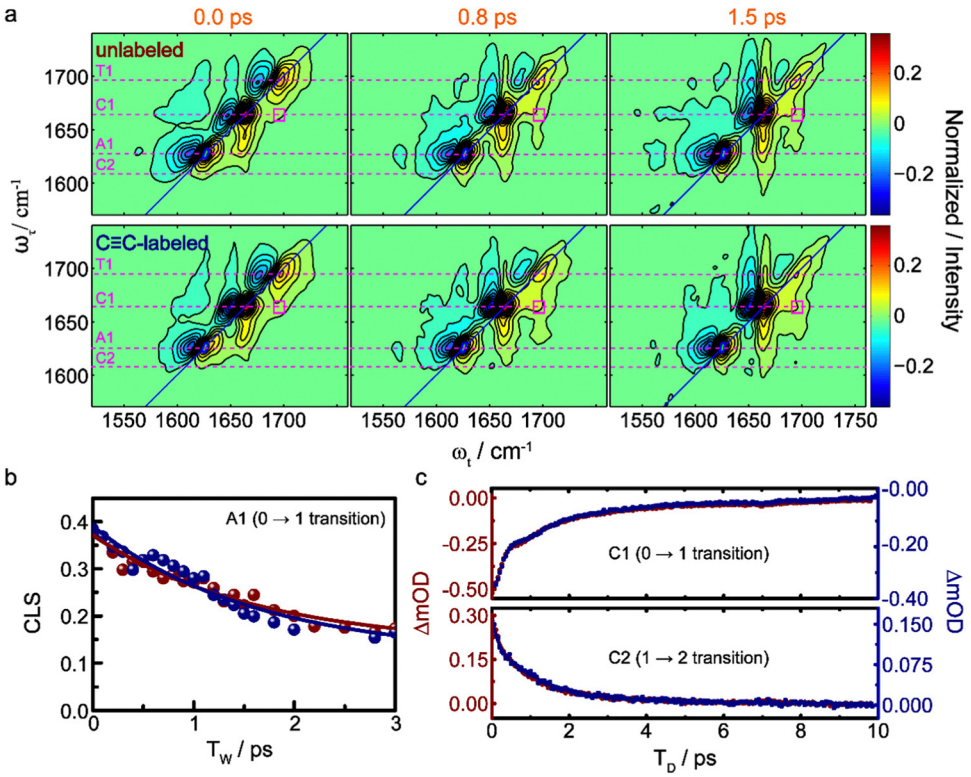

Fig. 6 (a) Waiting-time dependent 2D IR spectra of the folded structure of the unlabeled (top row) and the C≡C-labeled i-motif (bottom row). Dashed lines indicate the values of ω_τ for three prominent diagonal peaks of A1, C1, T1 and that for a shoulder peak C2, peaked at 1625 cm^{-1}, 1665 cm^{-1}, 1689 cm^{-1} and 1609 cm^{-1}, respectively. Purple rectangles indicate the off-diagonal cross peaks between C1 and T1 modes. (b) CLS of the A1 band ($0 \rightarrow 1$ transition) for the unlabeled case (wine) and C≡C-labeled case (navy). (c) Selected delay-time dependent dynamics for the unlabeled case (wine) and the C≡C-labeled case (navy). Probing ω_τ positions are 1665 cm^{-1} for C1 ($0 \rightarrow 1$ transition), 1603 cm^{-1} for C2 ($1 \rightarrow 2$ transition), and 1625 cm^{-1} for A1 ($0 \rightarrow 1$ transition). The peak labeling is described in Fig. 2. In (b), solid curves represent fittings with single exponential function. In (c), solid curves represent fittings with di-exponential function.

(Fig. 6a bottom row) and the unlabeled strand (Fig. 6a top row), which is so at varying waiting times. However, it should be noted that the 2D line shape changes as a function of the waiting time (from left to right panels of Fig. 6a), indicating the evolution of vibrational frequency (structural dynamics).

2D IR spectral line shape of the diagonal peaks changing with T_w is a process called spectral diffusion,[33,60–62] which provides a direct measurement of the inhomogeneity of a given vibration mode caused by the electric field involving both the solvent and local structure. The spectral diffusion dynamics can be extracted from the time-dependent 2D IR diagonal signal using inverse center-line slope (CLS) method that is defined as $\delta\omega_\tau/\delta\omega_t$. The spectral diffusion manifests the dynamics of the well-known frequency-frequency correlation function (FFCF).[62] The center-line was extracted for the 0 → 1 transition peaks of A1 (shown in Fig. 6a, marked with a blue dotted line at 1624–1630 cm^{-1}) which presents the local structure dynamics including solvent dynamics of the six adenines on average.

As shown in Fig. 6b, the CLS dynamics of two samples have almost the same initial amplitude value and the same unrelaxed residual value, indicating that the two samples have very similar inhomogeneity for the six adenines in a solvent environment as well as a local chemical environment, and also have similar local structural rigidity involving the six adenines. The CLS of two samples were fitted with a single exponential function with almost the same relaxation time constant (1.6 ps). This time constant reflects the averaged time scale of the local structural fluctuations (including solvent) around the six adenines. These adenine bases are evenly located on the three loops of the folded i-motif structure and are mainly solvent exposed (see Fig. S12, ESI†), hence the results suggest a relatively slower local dynamics than solvent water that typically has a time constant of 1.4–1.7 ps in bulk-like D_2O or H_2O.[63–67] The static component is related to the six adenines' structural fluctuations whose time constants are too long to measure in the experimental time window shown here. The time scale of fluctuations of the entire i-motif DNA structure is much longer than that of solvent water exchange dynamics when DNA is dissolved in aqueous solution. This static component would be observed if the time window is up to ~100 ps.[67,68] In summary, spectral diffusion dynamics shown in Fig. 6b indicates that there is no difference in the local structure dynamics of six adenines on average and solvent dynamics between the unlabeled and C≡C-labeled strands at the folded state.

From the magic-angle pump–probe spectra (Fig. S14, ESI†), population relaxation of the C=O stretching modes in these bases can be examined. For example, two vibrational relaxation dynamics of 0 → 1 transition peaks of C1 and 1 → 2 transition peaks of C2 are shown in Fig. 6c. The selected two transitions dynamics were fitted with a bi-exponential function and gave similar relaxation time constants. The dynamics fitting parameters are shown in Table S3 (ESI†). It was found that these dynamics show no much difference between the unlabeled and C≡C-labeled strands. These results indicate that the vibrational energy dissipation pathways of the vibrationally excited C=O modes in the i-motif DNA not affected by the C≡C-labeling folded strand are almost the same at each mode. Quite similar vibrational relaxations between the unlabeled and labeled i-motif DNA were also observed in other probing frequencies (data not shown).

To sum up, the extrinsic C≡C probe tagged on C_1 was found to have a negligible perturbation in the equilibrium structural transition process, local structural solvent dynamics and structural flexibility of the i-motif DNA. To further examine the extent of perturbations in the local structural dynamics from the C≡C probe, ultrafast infrared spectra of the partially folded-state structure of two strands dissolved in pH* 7.6 DPBS buffer solution were also collected. The spectra and related dynamics are shown in Fig. S15 (ESI†) and the fitting parameters for the dynamics are collected in Table S3 (ESI†). There was also no difference in all the corresponding dynamics between the unlabeled and C≡C-labeled strands. Thus, it is believed that the C≡C probe has a negligible perturbation in the local structure/solvent dynamics of the i-motif DNA even though the C≡C probe seems to have a large steric hindrance effect and hydrophobic effect. It appears to be more optimistic when a single C≡C probe is tagged on the major grooves and extends outward edge (less crowed area) of a DNA double helix or a highly ordered helical structure such as the i-motif DNA. Of course, our infrared spectroscopy has certain limitations and more sophisticated experiments should be carried out to further explore the perturbation induced by the C≡C probe.[69] Here, since the unfolding event occurred particularly on the local site probed by the C≡C label is found to be unlikely influenced by the structural perturbations from the probe itself, such a label is believed to have certain applicability and practicability. It should be noted that in a recent work of Tokmakoff and coworkers,[26] 2D IR spectroscopy in combination with ns T-jump was used to probe the unfolding dynamics of another i-motif DNA sequence 5′-CCCTTTCCCTTTCCCTTTCCC-3′ (C3T3) on the ms to second time scale. In their work, the C=O stretching mode (and ring thymine mode) can be used directly as the structural probe, which allows either global or local structural dynamics to be followed by 2D IR spectroscopy. In our work reported here, a site-specific, extrinsic IR probe (*i.e.*, the C≡C probe) was added so that local dynamics can be followed in a spectral window that does not have any intrinsic molecular vibration of DNA.

4. Concluding remarks

In this work, a site-specific thermal unfolding process of the i-motif DNA labeled by a C≡C probe on terminal cytosine (C_1) has been examined using temperature-dependent FTIR spectroscopy, in combination with quantum chemistry calculations. Temperature-dependent IR results indicate that the spectral features in both C=O/C=C stretching and the labeled C≡C stretching modes can be understood using a typical two-state model of the conformational transformation of DNA.

The extrinsic C≡C probe can be used to monitor the unfolding process of the i-motif DNA. The change of the

C≡C stretching frequency (and intensity) is directly related to the hemi-protonated base pair C_1–C_{13} breaking process and the protonated/non-protonated status of C_1 under its thermal unfolding process. The local T_m derived from the C≡C stretch (*ca.* 61.4 °C on average) is found to be slightly lower than that of the global T_m (*ca.* 63.1 °C on average), indicating that the C_1–C_{13} breaking process may be in the initial step of the denaturation. In addition, the local-site transition ΔH_m^{vH} exceeds 60% of that of the global transition, which implies that the C_1–C_{13} breaking process may be in the rate-limiting step of the denaturation and the remaining base pairs' break quickly follows.

Simulated IR spectra of the C≡C stretch of the C≡C-labeled hemi-protonated dimer and protonated/non-protonated monomer demonstrate that protons are more likely located on the C_1 side of the hemi-protonated base pair of C_1–C_{13}, so that C_1 remains to be protonated upon the breakage of the C_1–C_{13} link. The C≡C probe can successfully report the protonation status of site-specific nucleobase during the unfolding process of the i-motif DNA; the forming and breaking processes of the hemi-protonated base pair C_1–C_{13} lead to blue and red shifts in the C≡C stretching frequency, while the protonation and deprotonation processes of C_1 lead to a transition intensity decrease and increase, respectively, in the C≡C stretching mode.

Our ultrafast infrared spectroscopic results indicate that the extrinsic C≡C probe tagged on the i-motif DNA has little perturbation in the steady-state structural formation and transformation, and has little perturbation in the local structural dynamics, solvent dynamics and structural flexibility for the folded and partially folded i-motif DNAs. This may be because that the C≡C probe extends toward the major groove or the outside of the i-motif structure and avoids steric hindrance. Since there is no new short-range polar interaction (such as hydrogen-bonding interaction) introduced by the C≡C probe, it may become an advantageous structural and dynamics reporter for DNA. However, further experiments of the C≡C group labeling on other nucleobase sites and direct monitoring of the associated unfolding events are needed to verify the hypothesis. In addition, the proposed thermal unfolding model of the i-motif DNA from this work appears to be reasonable and generally agrees with that of pH-induced unfolding reported previously. Thus, our work demonstrated that the C≡C probe can be successfully used to monitor the site-specific unfolding process of the i-motif DNA for the first time. It should be generally applicable to the study of the thermal stability of DNA chains using infrared spectroscopy.

Conflicts of interest

There are no conflicts to declare.

Acknowledgements

Financial support from the National Natural Science Foundation of China (21973102, 21573243 and 21327802 to J. W.) is greatly acknowledged.

References

1 H. A. Day, P. Pavlou and Z. A. Waller, *Bioorg. Med. Chem.*, 2014, **22**, 4407–4418.
2 T. A. Brooks, S. Kendrick and L. Hurley, *FEBS J.*, 2010, **277**, 3459–3469.
3 M. Debnath, S. Ghosh, A. Chauhan, R. Paul, K. Bhattacharyya and J. Dash, *Chem. Sci.*, 2017, **8**, 7448–7456.
4 H. Abou Assi, M. Garavis, C. Gonzalez and M. J. Damha, *Nucleic Acids Res.*, 2018, **46**, 8038–8056.
5 M. Zeraati, D. B. Langley, P. Schofield, A. L. Moye, R. Rouet, W. E. Hughes, T. M. Bryan, M. E. Dinger and D. Christ, *Nat. Chem.*, 2018, **10**, 631–637.
6 S. Modi, M. G. Swetha, D. Goswami, G. D. Gupta, S. Mayor and Y. Krishnan, *Nat. Nanotechnol.*, 2009, **4**, 325–330.
7 H. Liu and D. Liu, *Chem. Commun.*, 2009, 2625–2636, DOI: **10.1039/b822719e**.
8 J. A. Kretzmann, K. L. Irving, N. M. Smith and C. W. Evans, *NAR Cancer*, 2021, **3**, zcab048.
9 S. L. Brown and S. Kendrick, *Pharmaceuticals*, 2021, **14**, 96.
10 C. Wang, Z. Huang, Y. Lin, J. Ren and X. Qu, *Adv. Mater.*, 2010, **22**, 2792–2798.
11 D. Liu, E. Cheng and Z. Yang, *NPG Asia Mater.*, 2011, **3**, 109–114.
12 M. Cheng, J. Chen, H. Ju, J. Zhou and J. L. Mergny, *J. Am. Chem. Soc.*, 2021, **143**, 7792–7807.
13 J. L. Leroy, *Nucleic Acids Res.*, 2009, **37**, 4127–4134.
14 A. L. Lieblein, J. Buck, K. Schlepckow, B. Furtig and H. Schwalbe, *Angew. Chem., Int. Ed.*, 2012, **51**, 250–253.
15 J. Choi, S. Kim, T. Tachikawa, M. Fujitsuka and T. Majima, *J. Am. Chem. Soc.*, 2011, **133**, 16146–16153.
16 C. Chen, M. Li, Y. Xing, Y. Li, C. C. Joedecke, J. Jin, Z. Yang and D. Liu, *Langmuir*, 2012, **28**, 17743–17748.
17 G. Mata and N. W. Luedtke, *J. Am. Chem. Soc.*, 2015, **137**, 699–707.
18 Y. Mao and J. Zhang, *J. Am. Chem. Soc.*, 2012, **134**, 631–639.
19 A. L. Lieblein, M. Kramer, A. Dreuw, B. Furtig and H. Schwalbe, *Angew. Chem., Int. Ed.*, 2012, **51**, 4067–4070.
20 J. Smiatek and A. Heuer, *RSC Adv.*, 2014, **4**, 17110–17113.
21 J. Smiatek, C. Chen, D. Liu and A. Heuer, *J. Phys. Chem. B*, 2011, **115**, 13788–13795.
22 J. Somkuti, O. R. Molnar and L. Smeller, *Phys. Chem. Chem. Phys.*, 2020, **22**, 23816–23823.
23 A. Ghosh, J. S. Ostrander and M. T. Zanni, *Chem. Rev.*, 2017, **117**, 10726–10759.
24 P. J. Sanstead, P. Stevenson and A. Tokmakoff, *J. Am. Chem. Soc.*, 2016, **138**, 11792–11801.
25 Y. Xu, R. Oyola and F. Gai, *J. Am. Chem. Soc.*, 2003, **125**, 15388–15394.
26 B. Ashwood, N. H. C. Lewis, P. J. Sanstead and A. Tokmakoff, *J. Phys. Chem. B*, 2020, **124**, 8665–8677.
27 M. S. Jones, B. Ashwood, A. Tokmakoff and A. L. Ferguson, *J. Am. Chem. Soc.*, 2021, **143**, 17395–17411.
28 H. Taskent-Sezgin, J. Chung, P. S. Banerjee, S. Nagarajan, R. B. Dyer, I. Carrico and D. P. Raleigh, *Angew. Chem., Int. Ed.*, 2010, **122**, 7635–7637.

29 H. Kim and M. Cho, *Chem. Rev.*, 2013, **113**, 5817–5847.
30 J. Ma, I. M. Pazos, W. Zhang, R. M. Culik and F. Gai, *Annu. Rev. Phys. Chem.*, 2015, **66**, 357–377.
31 R. Adhikary, J. Zimmermann and F. E. Romesberg, *Chem. Rev.*, 2017, **117**, 1927–1969.
32 R. Itaya, W. Idei, T. Nakamura, T. Nishihara, R. Kurihara, A. Okamoto and K. Tanabe, *ACS Omega*, 2021, **6**, 31595–31604.
33 T. Dong, P. Yu, J. Zhao and J. Wang, *Phys. Chem. Chem. Phys.*, 2022, **24**, 29988–29998.
34 S. Carson, J. Wilson, A. Aksimentiev, P. R. Weigele and M. Wanunu, *Nucleic Acids Res.*, 2016, **44**, 2085–2092.
35 T. T. Ngo, J. Yoo, Q. Dai, Q. Zhang, C. He, A. Aksimentiev and T. Ha, *Nat. Commun.*, 2016, **7**, 10813.
36 X. Teng and W. Hwang, *Biophys. J.*, 2018, **114**, 1791–1803.
37 S. A. Ingale, H. Mei, P. Leonard and F. Seela, *J. Org. Chem.*, 2013, **78**, 11271–11282.
38 A. T. Phan, M. Guéron and J.-L. Leroy, *J. Mol. Biol.*, 2000, **299**, 123–144.
39 D. B. Strasfeld, S. H. Shim and M. T. Zanni, *Phys. Rev. Lett.*, 2007, **99**, 038102.
40 S. H. Shim and M. T. Zanni, *Phys. Chem. Chem. Phys.*, 2009, **11**, 748–761.
41 M. J. Frish, G. W. Trucks, H. B. Schlegel, G. E. Scuseria, M. A. Robb, J. R. Cheeseman, G. Scalmani, V. Barone, B. Mennucci and G. A. Paterson, *Gaussian 09, Revision A. 02*, Gaussian, Inc., Pittsburgh PA, 2009.
42 D. Reinstädler, H. Fabian, J. Backmann and D. Naumann, *Biochemistry*, 1996, **35**, 15822–15830.
43 P. Renati, Z. Kovacs, A. De Ninno and R. Tsenkova, *J. Mol. Liq.*, 2019, **292**, 111449.
44 M. Bukleski, S. Dimitrovska-Lazova, V. Makrievski and S. Aleksovska, *Spectrochim. Acta, Part A*, 2020, **231**, 118118.
45 M. Bukleski, S. Dimitrovska-Lazova and S. Aleksovska, *Spectrochim. Acta, Part A*, 2022, **266**, 120462.
46 Z. A. Piskulich and W. H. Thompson, *J. Phys. Chem. Lett.*, 2020, **11**, 7762–7768.
47 D. Tsankov, M. Krasteva, V. Andrushchenko, J. Van De Sande and H. Wieser, *Biophys. Chem.*, 2006, **119**, 1–6.
48 J. Somkuti, M. Houska and L. Smeller, *Eur. Biophys. J.*, 2011, **40**, 143–151.
49 M. H. Brumano, E. Rogana and H. E. Swaisgood, *Arch. Biochem. Biophys.*, 2000, **382**, 57–62.
50 D. Du, M. J. Tucker and F. Gai, *Biochemistry*, 2006, **45**, 2668–2678.
51 M. R. Bunagan, J. Gao, J. W. Kelly and F. Gai, *J. Am. Chem. Soc.*, 2009, **131**, 7470–7476.
52 M. McKim, A. Buxton, C. Johnson, A. Metz and R. D. Sheardy, *J. Phys. Chem. B*, 2016, **120**, 7652–7661.
53 S. D. Stelea, P. Pancoska, A. S. Benight and T. A. Keiderling, *Protein Sci.*, 2001, **10**, 970–978.
54 S. M. Reilly, R. K. Morgan, T. A. Brooks and R. M. Wadkins, *Biochemistry*, 2015, **54**, 1364–1370.
55 M. Kaushik, N. Suehl and L. A. Marky, *Biophys. Chem.*, 2007, **126**, 154–164.
56 D. T. Leeson, F. Gai, H. M. Rodriguez, L. M. Gregoret and R. B. Dyer, *Proc. Natl. Acad. Sci. U. S. A.*, 2000, **97**, 2527–2532.
57 D. Du, Y. Zhu, C.-Y. Huang and F. Gai, *Proc. Natl. Acad. Sci. U. S. A.*, 2004, **101**, 15915–15920.
58 H. Rahaman, M. K. A. Khan, M. I. Hassan, A. Islam, A. A. Moosavi-Movahedi and F. Ahmad, *J. Chem. Thermodyn.*, 2013, **58**, 351–358.
59 R. D. Johnson III and E. NIST, *Computational chemistry comparison and benchmark database*, 2013.
60 H. Ishikawa, S. Kim, K. Kwak, K. Wakasugi and M. D. Fayer, *Proc. Natl. Acad. Sci. U. S. A.*, 2007, **104**, 19309–19314.
61 K. Kwak, D. E. Rosenfeld and M. D. Fayer, *J. Chem. Phys.*, 2008, **128**, 204505.
62 D. Li, F. Yang, C. Han, J. Zhao and J. Wang, *J. Phys. Chem. Lett.*, 2012, **3**, 3665–3670.
63 S. Park, K. Kwak and M. D. Fayer, *Laser Phys. Lett.*, 2007, **4**, 704–718.
64 R. Yuan, C. Yan, A. Tamimi and M. D. Fayer, *J. Phys. Chem. B*, 2015, **119**, 13407–13415.
65 S. Park and M. D. Fayer, *Proc. Natl. Acad. Sci. U. S. A.*, 2007, **104**, 16731–16738.
66 S. A. Yamada, W. H. Thompson and M. D. Fayer, *J. Chem. Phys.*, 2017, **146**, 234501.
67 J. T. King and K. J. Kubarych, *J. Am. Chem. Soc.*, 2012, **134**, 18705–18712.
68 J. K. Chung, M. C. Thielges, S. E. Bowman, K. L. Bren and M. D. Fayer, *J. Am. Chem. Soc.*, 2011, **133**, 6681–6691.
69 B. Ashwood, M. S. Jones, A. L. Ferguson and A. Tokmakoff, *Proc. Natl. Acad. Sci. U. S. A.*, 2023, **120**, e2219124120.

